JGR Space Physics

RESEARCH ARTICLE
10.1029/2019JA026678

Special Section:
Long-term changes and Trends in the Middle and Upper Atmosphere

Whole Atmosphere Climate Change: Dependence on Solar Activity

Stanley C. Solomon[1], Han-Li Liu[1], Daniel R. Marsh[1,2], Joseph M. McInerney[1], Liying Qian[1], and Francis M. Vitt[1,2]

[1]High Altitude Observatory, National Center for Atmospheric Research, Boulder, CO, USA, [2]Atmospheric Chemistry and Modeling, National Center for Atmospheric Research, Boulder, CO, USA

Key Points:
- We performed whole-atmosphere climate change simulations, for solar maximum conditions, and compared them to previous work for solar minimum
- In the thermosphere and ionosphere, anthropogenic climate change at solar maximum is smaller than at solar minimum, in these simulations
- The solar cycle effect on temperature ranges from 500 K in the thermosphere to near zero at the tropopause

Correspondence to:
S. C. Solomon,
stans@ucar.edu

Citation:
Solomon, S. C., Liu, H.-L., Marsh, D. R., McInerney, J. M., Qian, L., & Vitt, F. M. (2019). Whole atmosphere climate change: Dependence on solar activity. *Journal of Geophysical Research: Space Physics*, *124*, 3799–3809. https://doi.org/10.1029/2019JA026678

Received 1 MAR 2019
Accepted 25 APR 2019
Accepted article online 30 APR 2019
Published online 28 MAY 2019

Abstract We conducted global simulations of temperature change due to anthropogenic trace gas emissions, which extended from the surface, through the thermosphere and ionosphere, to the exobase. These simulations were done under solar maximum conditions, in order to compare the effect of the solar cycle on global change to previous work using solar minimum conditions. The Whole Atmosphere Community Climate Model-eXtended was employed in this study. As in previous work, lower atmosphere warming, due to increasing anthropogenic gases, is accompanied by upper atmosphere cooling, starting in the lower stratosphere, and becoming dramatic, almost 2 K per decade for the global mean annual mean, in the thermosphere. This thermospheric cooling, and consequent reduction in density, is less than the almost 3 K per decade for solar minimum conditions calculated in previous simulations. This dependence of global change on solar activity conditions is due to solar-driven increases in radiationally active gases other than carbon dioxide, such as nitric oxide. An ancillary result of these and previous simulations is an estimate of the solar cycle effect on temperatures as a function of altitude. These simulations used modest, five-member, ensembles, and measured sea surface temperatures rather than a fully coupled ocean model, so any solar cycle effects were not statistically significant in the lower troposphere. Temperature change from solar minimum to maximum increased from near zero at the tropopause to about 1 K at the stratopause, to approximately 500 K in the upper thermosphere, commensurate with the empirical evidence, and previous numerical models.

Plain Language Summary We conducted global simulations of temperature change due to emissions of trace gases due to human activity, which extended from the surface, throughout the atmosphere, to space. These simulations were done under conditions of high solar activity, in order to compare the effect of the solar cycle to previous work using low solar activity. The Whole Atmosphere Community Climate Model-eXtended was employed. As in previous work, lower atmosphere warming, due to increasing emissions of greenhouse gases, is accompanied by upper atmosphere cooling, starting in the lower stratosphere, and becoming dramatic, almost 2 K per decade on average, above 100-km altitude. This upper atmosphere cooling, and consequent reduction in density, is less than the almost 3 K per decade for low solar activity conditions calculated in previous simulations. The dependence of global change on solar activity is due to solar-driven increases in other gases that cool the thermosphere, so greenhouse gases such as carbon dioxide have less effect. An ancillary result is an estimate of the solar cycle effect on temperatures as a function of altitude, which increased from near zero at about 15 km to approximately 500 K at about 400 km, commensurate with previous work.

1. Introduction

The *greenhouse effect* warms the lower atmosphere, surface, and oceans due to the absorption and trapping of infrared radiation by atmospheric trace gases, including carbon dioxide (CO_2), water vapor (H_2O), methane (CH_4), and ozone (O_3). Some of these, particularly CO_2 and CH_4, have increased during the past century as the result of human activity, causing surface and tropospheric temperatures to rise by ~1 K globally. Increases in these same gases, especially CO_2, have paradoxically caused the upper atmosphere to cool. This is because as the atmosphere becomes transparent to infrared radiation with increasing altitude, energy from collisional excitation followed by infrared emission is able to escape to space. Theory and modeling of this phenomenon (e.g., Akmaev, 2012; Akmaev et al., 2006; Akmaev & Fomichev, 2000; Brasseur & Hitchman, 1988; Dickinson, 1984; Fels et al., 1980; Fomichev et al., 2007;

Garcia et al., 2007; Lübken et al., 2013; Qian et al., 2006, 2013, 2014; Roble & Dickinson, 1989; Solomon et al., 2015; Solomon, Liu, et al., 2018) have established the mechanisms and global effects throughout the stratosphere-mesosphere-thermosphere-ionosphere and led to some convergence with observational evidence; see the reviews by, for example, Beig et al., 2003; Laštovička, 2017; Laštovička et al., 2006, 2012; Qian et al., 2011, and references within. One effect of this cooling is to cause the atmosphere to contract as its scale height decreases, so that it is lower in density at a constant altitude. This effect is small below the stratopause but becomes large in the mesosphere and especially in the thermosphere. Thus, the decrease in temperature, and thus density, is discoverable by observing long-term trends in the orbital elements of near-Earth satellites, which are affected by atmospheric drag that is systematically decreasing over time (Emmert, 2015; Emmert et al., 2004, 2008; Keating et al., 2000; Marcos et al., 2005; Saunders et al., 2011).

These gradual changes are superimposed on variation due to solar activity in all of its forms. The amplitude of the solar-driven variation increases with altitude, culminating in the upper thermosphere with factor-of-2 variation in temperature and order-of-magnitude variation in density (e.g., Qian & Solomon, 2012). Just as interannual variation and anthropogenic change makes it almost impossible to discern the very weak signal of solar variability effects at the surface, the solar, geomagnetic, and seasonal variation of the thermosphere make it difficult to observationally quantify the slow cooling due to increasing levels of greenhouse gases. From the modeling perspective, the task is simplified by our ability to switch on and off the variability of various boundary conditions and perform analysis of model forcing terms. Observational analysis has no such luxury, as it is required to deal with the single instance of objective reality as it presents itself to our limited instrumentation.

We have now performed new model runs simulating global change throughout the atmosphere, using the Whole Atmosphere Community Climate Model-eXtended, similar to previous ones (Solomon, Liu, et al., 2018), but under solar maximum conditions instead of solar minimum. This enables us to further explore the extent to which anthropogenic change in the upper atmosphere is modulated by solar activity. This integrated approach, with a single model, advances earlier work using different models for different regions. An ancillary result is an estimate of the solar cycle effect throughout the atmosphere.

2. Model Simulations

2.1. Model Overview

The Community Atmosphere Model (CAM) is the atmospheric component of the NCAR Community Earth System Model (CESM; Hurrell et al., 2013). Its extension, the Whole Atmosphere Community Climate Model (WACCM), uses the same column physics and the same dynamical core and can be coupled to ocean, land, and ice models in the same way, but it extends to 140-km altitude. However, since it does not consider major species diffusion or independent ion transport and is subject to the influence of its empirical upper boundary condition down to ~120 km, it cannot be reliably used above that altitude. Therefore, WACCM-eXtended has been developed in order to calculate the global neutral winds, temperatures, densities, and composition, ion drifts, density, and composition, ion and electron temperatures, and electric potential, from the surface to the exobase. The model uses a hydrostatic log-pressure coordinate system and extends above ~600 km in altitude (depending on solar activity). WACCM-X v. 2.0 uses a horizontal grid that is 1.9° × 2.5° in latitude and longitude and 0.25 scale height vertical resolution above 1 hPa.

WACCM-X v. 2.0 is based on CAM4 and WACCM4 physics and chemistry (Marsh et al., 2013; Neale et al., 2013), as released in CESM v. 1.0. The simulations shown here were conducted using internal version number 5.4.166, which, for WACCM-X, is functionally the same as v. 5.4.99, which was used in recent work (Solomon, Liu, et al., 2018). For descriptions of the original formulation of WACCM and WACCM-X, and further discussion of chemistry, radiative transfer, and other forcings such as volcanic aerosols, see Marsh et al. (2007, 2013) and Liu et al. (2010). Radiative cooling mechanisms in the thermosphere include CO_2, NO collisional excitation, and $O(^3P)$ fine structure emission. Recent developments, resulting in the release of WACCM-X v. 2.0 as an extended element of CESM v. 2.0, include high-altitude adaptations to the dynamical core, interactive ionospheric electrodynamics and transport, and metastable ion chemistry, which are described in Liu et al. (2018).

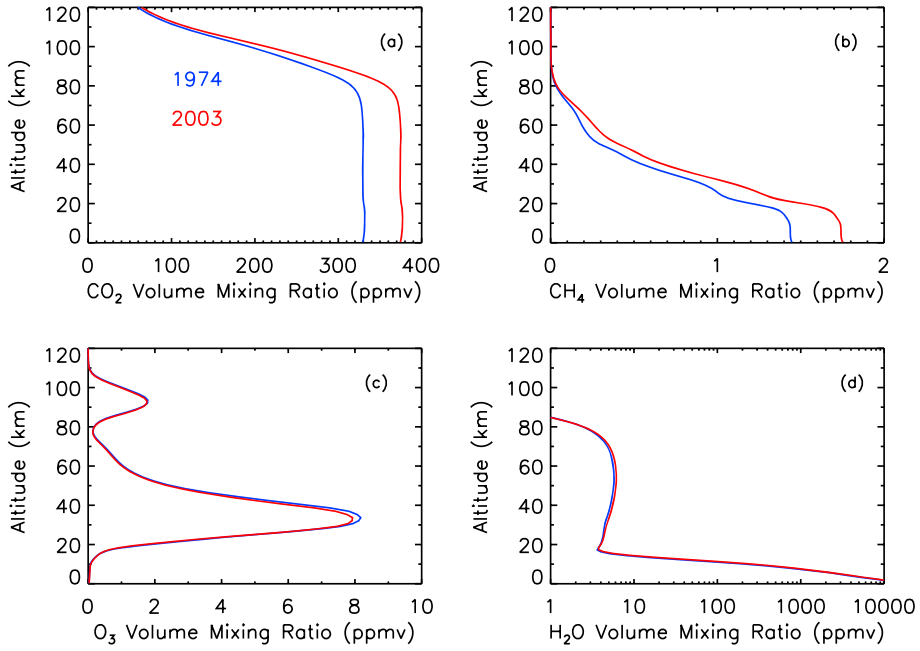

Figure 1. Global mean annual mean altitude profiles of anthropogenic gases for the two epochs. Blue: 1974. Red: 2003. (a) CO_2 volume mixing ratio (ppmv). (b) Methane volume mixing ratio (ppmv). (c) Ozone volume mixing ratio (ppmv). (d) Water vapor volume mixing ratio (ppmv).

2.2. Global Change Simulations

The model simulations were performed using WACCM-X v. 2.0 in free-running climate mode, which allows the model to generate its own internal variability due to *weather*, but are not specifically representative of a particular day. Previous work (Solomon, Liu, et al., 2018) simulated solar minimum conditions, so that solar and geomagnetic variations were controlled and climate change could be isolated. This work uses the same approach, but instead of a solar spectrum representative of solar minimum, with solar 10.7-cm radio flux ($F_{10.7}$) index of 70, and geomagnetic conditions represented by a planetary amplitude $K_p = 0.3$, we employed a solar spectrum and geomagnetic conditions representative of solar maximum ($F_{10.7} = 200$ and $K_p = 3.0$). We conducted 5-year simulations for the years 1972–1976, and 2001–2005, which serves as a small ensemble of similar years, in order to evaluate how interannual variability affects the results and to enable the calculation of ensemble means. The model was *spun up* for a year under solar minimum conditions for each epoch, and then for another 3 months under solar maximum conditions, before the start of the study interval, in order to equilibrate the atmospheric response. An empirical stratospheric quasi-biennial oscillation and observed sea surface temperatures (Huang et al., 2015, 2017) were imposed. Lower boundary conditions specifying time-dependent trace gas inputs were the same as the standard reference case employed in the Chemistry Climate Model Initiative (Eyring et al., 2013). Figure 1 shows the altitude dependence of the key trace constituents CO_2, CH_4, H_2O, and O_3, averaged over each of the two ensembles. CO_2 and CH_4 are different because the lower boundary condition changed; H_2O changes (very slightly) in response to the internal chemistry and dynamics of the model, and O_3 decreases because of increased chlorofluorocarbon (CFC) fluxes at the lower boundary. Note that this interval was chosen in part because it roughly corresponds to the most rapid period of O_3 depletion; around the year 2000, global mean column O_3 leveled off, presumably due to decreased CFC emissions.

Annual mean global fields of temperatures, densities, and heights were averaged from the monthly mean model output, zonal mean annual means were then derived, and 5-year zonal means were averaged from the individual years. Zonal mean temperature differences between the two epochs are shown in Figure 2.

Global means of the annual means, and then ensemble averages, were obtained from the zonal means using a cos (lat) weighting function. Global mean profiles, temperature changes, and density changes are shown in Figure 3. Figures 3a and 3b show temperature and density profiles versus the global mean geometric altitude.

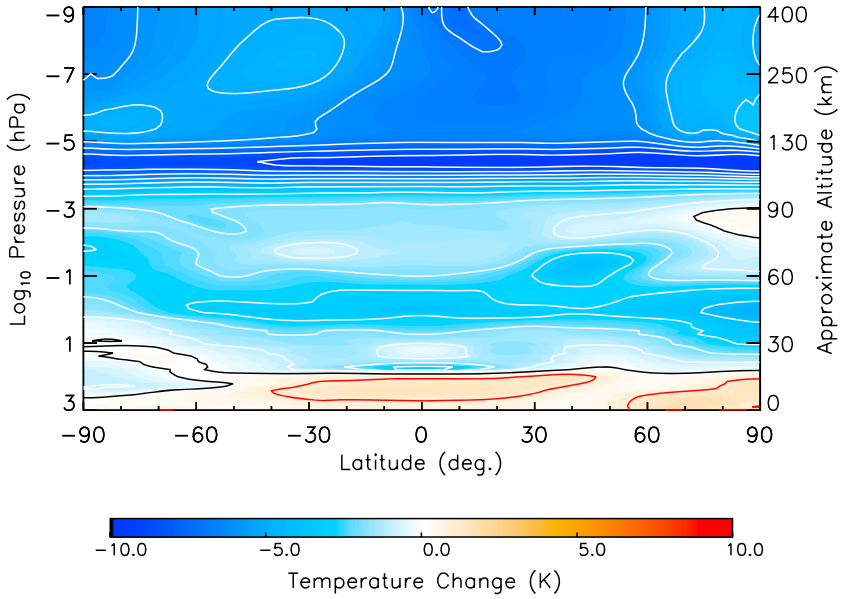

Figure 2. Model calculations of the zonal mean annual mean changes in temperature under high solar activity conditions, as a function of latitude and pressure, for the 29-year simulation period between 5-year ensembles (1972–1976 to 2001–2005). Negative contours, ranging from −9 to −1 K, with a 1-K interval, are shown in white; positive contours, at +1 and +2 K, are shown in red. The zero-change line is shown in black.

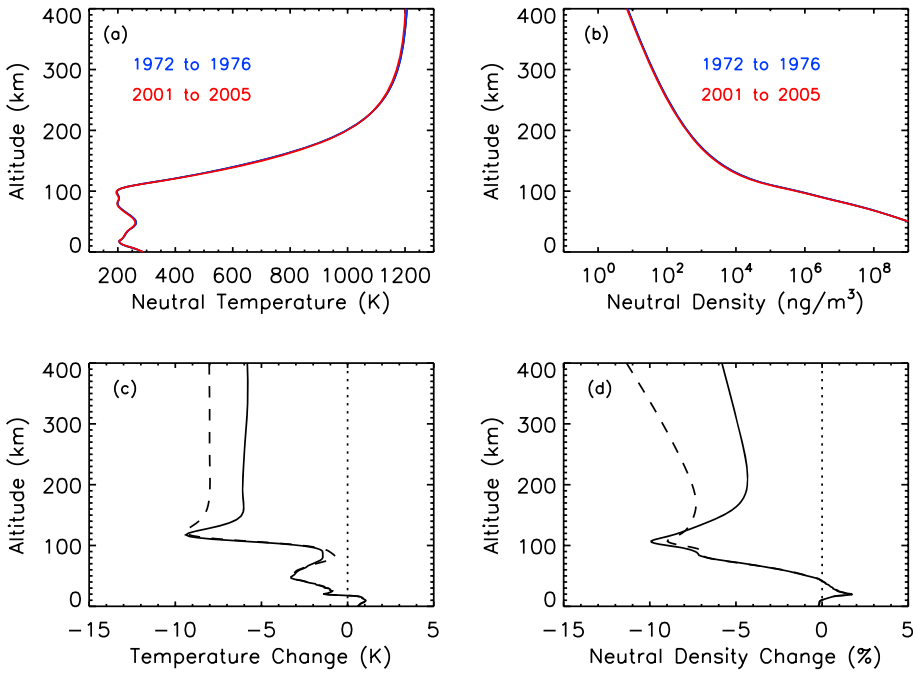

Figure 3. Model calculations of the global mean annual mean changes, under high solar activity conditions, over the 29-year period between 5-year ensembles (1972–1976 to 2001–2005), with CO_2 levels at the surface increasing from 330 to 373 ppmv. Note that the quantities shown in panels a, b, and d are calculated in actual altitude coordinates, but the temperature changes shown in panel c are calculated in pressure coordinates, and then referenced to the altitudes for those pressures in the 1972–1976 ensemble. (a) Temperature profiles as a function of altitude. Blue: 1972–1976 (T_1). Red: 2001–2005 (T_2). (b) Neutral mass density as a function of altitude. Blue: 1972–1976 (n_1). Red: 2001–2005 (n_2). (c) Temperature change as a function of altitude, T_2-T_1. Solid line: solar maximum conditions. Dashed line: solar minimum conditions (from Solomon, Liu, et al., 2018). (d) Neutral number density percent change as a function of altitude, $100(n_2\text{-}n_1)/n_1$. Solid line: solar maximum conditions. Dashed line: solar minimum conditions.

Table 1
Model Inputs and Key Results for High Solar Activity

Inputs	1972–1976	2001–2005	Change per decade
<CO_2> at surface	330 ppmv	375 ppmv	+16 ppmv
<CH_4> at surface	1.44 ppmv	1.74 ppmv	+0.10 ppmv
<CFC11 + CFC12> at surface	0.29 ppbv	0.79 ppbv	+0.17 ppbv
$F_{10.7}$ index	200	200	0
K_p index	3.0	3.0	0
Results	*1972–1976*	*2001–2005*	*Change per decade*
<T> at surface	287.8 K	288.4 K	+0.2 K
<T> at 10 km (266 hPa)	225.8 K	226.9 K	+0.4 K
<T> at tropopause	204.2 K	204.5 K	+0.1 K
<T> at stratopause	263.7 K	260.4 K	−1.1 K
<T> at mesopause	196.7 K	194.4 K	−0.8 K
<T> at 400 km	1,201.6 K	1,206.8 K	−1.8 K
<ρ> at 400 km (mass density)	7.23 ng/m^3	6.87 ng/m^3	−1.7%
<NmF_2> (peak ion density)	8.90×10^5 cm^{-3}	8.62×10^5 cm^{-3}	−1.2%
<hmF_2> (height of peak)	329 km	326 km	−1.0 km
<T_i> at hmF_2 (ion temperature)	1,208.1 K	1,201.0 K	−2.8 K

Figure 3c plots global mean temperature differences between the two epochs. The vertical coordinate in this panel is actually pressure but referenced to the 1972–1976 pressure surface mean altitude. For Figure 3d, density change is calculated at fixed altitude, with the results for 2001–2005 interpolated to the 1972–1976 altitude grid. The temperature and density changes at solar minimum, from Solomon, Liu, et al. (2018), are also plotted in Figures 3c and 3d (dashed lines), for comparison. Temperature and density changes at important altitude levels are shown in Table 1, converted into degrees Kelvin per decade.

There is considerable interannual variation in temperature throughout the atmosphere, as shown in Figure 4, which is the reason that multiyear model (or observational) ensembles are necessary to discern global change. Global mean annual mean temperature profiles, differenced relative to the 1972–1976 ensemble mean on pressure surfaces, are plotted against the 1972–1972 ensemble mean altitudes. Note that the model variance at the surface (and probably throughout the troposphere) is influenced by the use of observed sea surface temperatures but is nevertheless realistic. The year-to-year variation is largest, on a percentage basis, in the upper mesosphere, but is also noticeable in the thermosphere. We reiterate that these simulations use

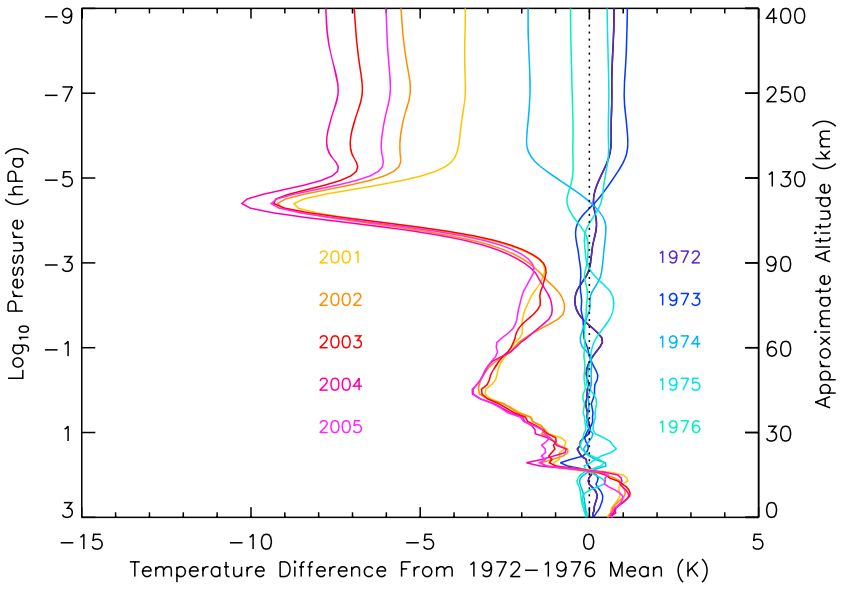

Figure 4. Interannual variability of global mean annual mean temperatures under constant high solar activity conditions. Temperature difference from mean of 1972 to 1976 simulations, as labeled.

solar and geomagnetic inputs that are artificially held constant, so that we can focus on the anthropogenic effects.

3. Discussion

3.1. Anthropogenic Changes

Below the mesopause, these results for solar maximum are similar to those of Solomon, Liu, et al. (2018) for solar minimum. This is as expected, since the primary gases controlling cooling and heating rates are weakly dependent on solar activity in that altitude region. Therefore, the comparisons to other modeling and observational work given in Solomon, Liu, et al. (2018) apply equally here. Near the mesopause itself, where the solar cycle variations in temperature become larger than trends introduced by anthropogenic change (or other forms of global change), the picture becomes somewhat complex, as long-term observations are difficult, and interannual variability is large. She et al. (2015) found a -2.8 ± 0.6 K/decade trend near 92 km in lidar data, significantly larger than estimated here; this is somewhat reduced in subsequent analysis by Yuan et al. (2018) that considers the seasonal and solar cycle effects, but this is for a single location, not a global average. For other observational work relevant to the mesosphere and mesopause, see the review by Laštovička (2017), which substantiates the uncertainties regarding this complex atmospheric region. Other model estimates, including Akmaev and Fomichev (2000), Fomichev et al. (2007), Garcia et al. (2007), Lübken et al. (2013), and Qian et al. (2019) are in general agreement with the WACCM-X simulations, finding mesopause-region trends to be fairly small.

At higher altitude, there is a far larger solar cycle effect on temperatures and densities, so the analysis becomes challenging. The seminal work by Keating et al. (2000) analyzed satellite drag data from solar minimum only, thereby hoping to remove external effects, finding ~ −5%/decade reduction in density at 400-km altitude. Emmert et al. (2004, 2008) found similar density trends for solar minimum conditions, but with the trend reducing to ~ −2%/decade at higher solar activity (cf., Figure 3 of Emmert et al., 2008). An additional analysis of satellite orbital elements by Saunders et al. (2011) only sorted the trends into minimum and moderate-to-high activity levels, yielding larger trends but similar amplitude. However, Emmert (2015) revised the earlier estimation of a solar cycle dependence on thermospheric trends, finding only that any solar cycle dependence is weak relative to the trend uncertainties. The basis for this was that as solar and geomagnetic activity have tended to decline over the past several cycles, it has become difficult to disentangle the relative effects of increasing CO_2 over the same time period. In particular, the minimum period between solar Cycles 23 and 24 had unusually low thermosphere and ionosphere densities, driven mostly by solar effects; see Emmert et al. (2010, 2014), Emmert, (2015), Solomon et al. (2010, 2011, 2013), Solomon, Qian, and Mannucci (2018), and references therein, for further discussion. This may have ramifications for the original Keating et al. (2000) estimate, as there may have been some progressive reduction in activity leading up to the Cycles 23–24 crash, although certainly not as dramatic.

From the modeling perspective, long-term trends should have some solar cycle dependence, since thermospheric cooling rates from other minor species, particularly nitric oxide (NO) but also atomic oxygen ($O(^3P)$), are much larger at solar maximum, unlike CO_2 cooling, which has a modest solar cycle dependence. Our past work (e.g., Qian et al., 2006, 2011, 2014; Solomon et al., 2015) found moderate temperature trend dependence on solar activity, and these simulations are no exception, but we agree that uncertainty regarding how the solar cycle is changing has an impact on observational efforts. Nevertheless, in Table 2 we provide a summary of model simulation and observational analyses of thermospheric density general conditions, for the two broad ranges utilized by Saunders et al. (2011), near-solar-minimum conditions and moderate-to-high activity, and also for overall average solar activity.

Trends in ionospheric parameters obtained from the model simulations results are also given in Table 1. The ion temperature T_i is similar to the neutral temperature up to the altitude h_mF_2 of the peak density of the F region N_mF_2, so observations of T_i by incoherent scatter radar should be a valuable way to monitor thermospheric climate change. Analysis of radar observations (e.g., Zhang et al., 2011, 2016; Zhang & Holt, 2013) has been larger than estimates based on satellite drag, as shown by Akmaev (2012), but may be influenced by secular decline in solar activity or variation of the magnetic field (Cnossen & Richmond, 2012). Recent work by Wang and Qian (2018) demonstrates that magnetic field evolution at the location of the Millstone Hill radar could be responsible for the large trends in T_i observed at that location.

Table 2
Observed and Modeled Trends in Thermospheric Density

Δ<ρ> at 400-km altitude	Low solar activity	Overall average solar activity	Moderate-to-high solar activity
Observations			
Keating et al. (2000)	−5%		
Marcos et al. (2005)		−1.7% to −2.4%	
Emmert et al. (2008)	−5.5 ± 1.4%		−2 ± 1%
Saunders et al. (2011)	−7%		−4%
Emmert (2015)		−2 ± 0.5%	
Models			
Roble and Dickinson (1989)		−3%	
Rishbeth and Roble (1992)		−2%	
Qian et al. (2006)	−2.5%	−1.7%	−0.8%
Akmaev et al. (2006), Akmaev and Fomichev (2000)*		−3 to −5%	−3 to −5%
Solomon et al. (2015)	−4.9%		−2.0%
Solomon, Liu, et al. (2018)	−3.9%		
This Work			−1.7%

*at 200-km altitude.

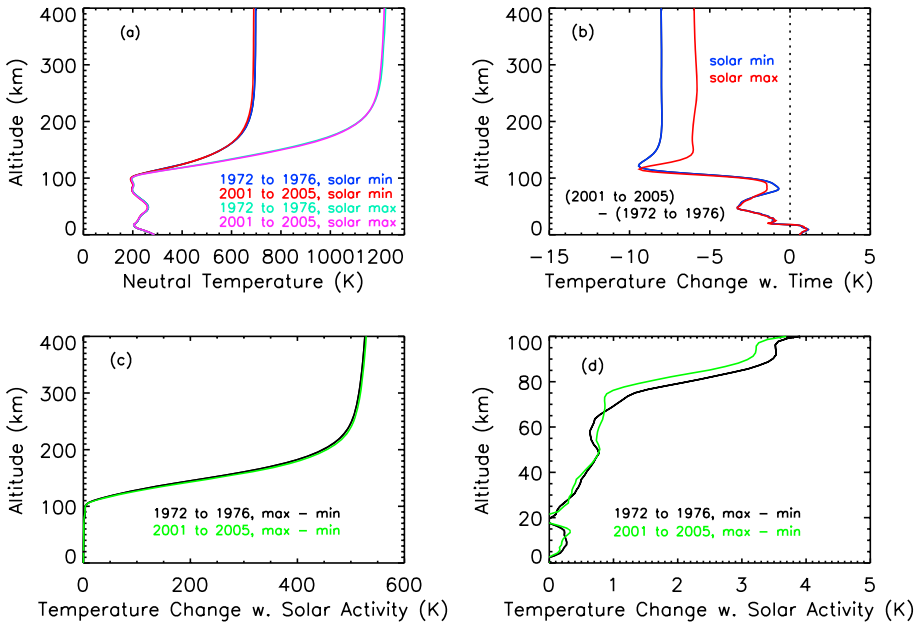

Figure 5. Model calculations of the anthropogenic and solar cycle variation in global mean annual mean temperature. Note that the temperature profiles shown in panel a are calculated in actual altitude coordinates, but the temperature changes shown in panel (b) are actually calculated in pressure coordinates, and then referenced to the altitudes for those pressures in the 1972–1976 ensemble. The temperature changes shown in panels (c) and (d) are also calculated in pressure coordinates, referenced to the altitude scale for the solar minimum case for each ensemble. (a) Temperature profiles as a function of altitude. Blue: 1972 to 1976 ensemble, solar minimum; red: 2001 to 2005 ensemble, solar minimum; cyan: 1972 to 1976 ensemble, solar maximum; magenta: 2001 to 2005 ensemble, solar maximum. (b) Temperature change between the two epochs. Blue: solar minimum conditions; red: solar maximum conditions. (c) Temperature change with solar activity. Black: solar max-solar min for the 1972 to 1976 ensemble; green: solar max-solar min for the 2001 to 2005 ensemble. (d) Same as (c) but with an expanded altitude scale to show the lower and middle atmosphere. Changes of less than 0.2°, below ~10 km, are not considered statistically significant for these modest ensemble sizes, and also note that lower troposphere temperatures are largely controlled by the use of measured sea surface temperatures as a lower boundary condition.

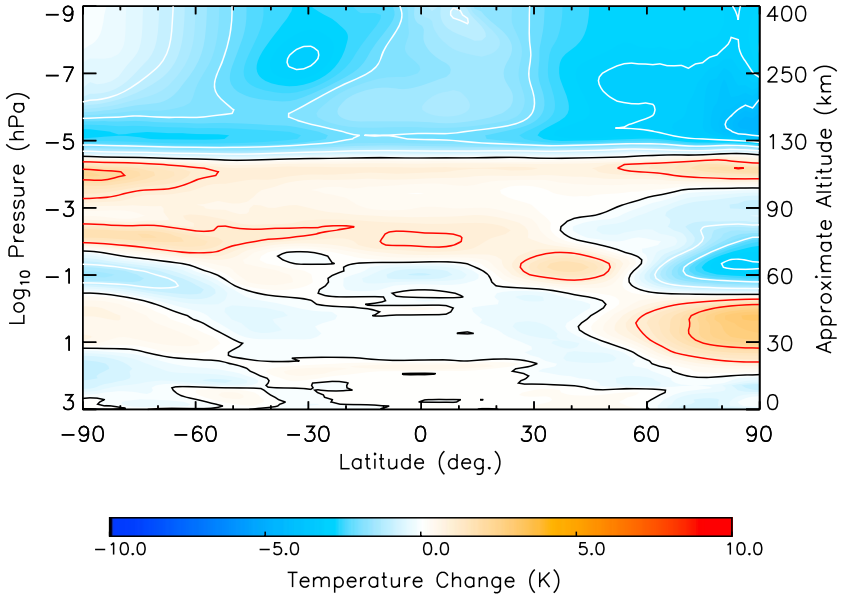

Figure 6. Model calculations of the differences between temperature change at high solar activity and at low solar activity, as a function of latitude and pressure, for the 29-year simulation period between 5-year ensembles, i.e., $[(2001\text{ to }2005)_{max} - (1972\text{ to }1976)_{max}] - [(2001\text{ to }2005)_{min} - (1972\text{ to }1976)_{min}]$. Negative contours, with a 1-K interval, are shown in white; positive contours are shown in red. The zero-difference line is shown in black. Negative (blue) regions are therefore where the time-dependent change is greater at solar minimum; positive (red) regions are where the time-dependent change is greater at solar maximum.

3.2. Solar Cycle Changes

An ancillary result of this study, when combined with the simulations conducted for Solomon, Liu, et al. (2018), is an estimate of the effect on the atmosphere of changes in solar spectral irradiance due to the 11-year solar cycle. In Solomon, Liu, et al. (2018), we conducted simulations using the same inputs shown in Table 1, except with $F_{10.7} = 70$ and $K_p = 0.3$. Solar spectral irradiance increases with solar activity, by more than a factor of 2 in the extreme ultraviolet, a few percent in the ultraviolet, and less than a part in a thousand in the visible and infrared. Since extreme-ultraviolet radiation is absorbed in the thermosphere, we expect large changes in temperature. Increased geomagnetic activity during solar maximum also plays a role. In the middle atmosphere, variability of ultraviolet radiation, and consequent changes in O_3, cause small solar-cycle effects on temperature. In the troposphere, the solar cycle effect on global mean temperature is uncertain, as it is much smaller than the upper atmosphere response.

In Figure 5a, we plot the global mean annual mean temperature profiles for each of the four five-member ensembles. In Figure 5b, the temperature change due to the different lower boundary condition for the two epochs is displayed, similar to Figure 3c, but for both the solar maximum case and the solar minimum case. Panels (c) and (d) of Figure 5 show the change with solar activity for each epoch. Note that the temperature profiles shown in panel (a) are calculated in geometric altitude coordinates, but the temperature change profiles shown in panel (b) are actually calculated in pressure coordinates, and then referenced to the altitudes for those pressures in the 1972–1976 ensemble. The temperature changes shown in panels (c) and (d) are also calculated in pressure coordinates, referenced to the solar minimum altitude scale for each ensemble. The thermospheric change seen in panel (c) is similar to empirical models (e.g., NRLMSISE-00; Picone et al., 2002) and previous work with numerical models (e.g., Qian & Solomon, 2012). In order to discern the much smaller middle atmosphere and lower atmosphere changes, panel (d) displays the same data on an expanded scale. The results here are similar to those of Marsh et al. (2007) using an earlier version of WACCM, but do show very small tropospheric changes. Increases of less than 0.2 K, below ~10 km, are not considered to be significant for these modest ensemble sizes, and also note that lower troposphere temperatures are largely controlled by the use of measured sea surface temperatures as a lower boundary condition. The similarity between the solar cycle effects for the two epochs shows that on a global mean bases, there is little interaction between anthropogenic and solar cycle effects in the troposphere, although there could be

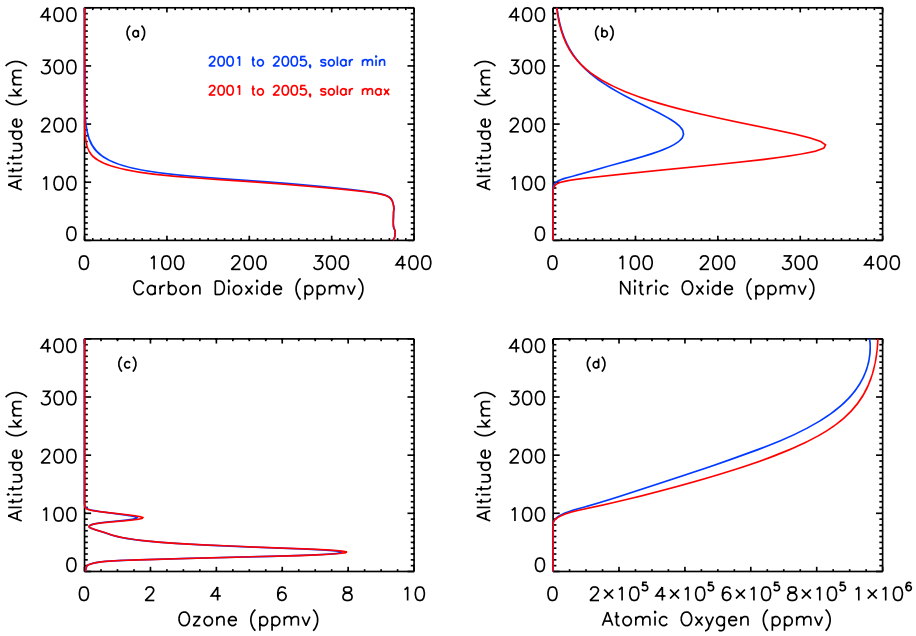

Figure 7. Global mean annual mean model altitude profiles of selected radiatively active species at solar minimum and solar maximum for the 2001 to 2005 epoch. Blue: solar minimum. Red: solar maximum. (a) CO_2 volume mixing ratio (ppmv). (b) Nitric oxide volume mixing ratio (ppmv). (c) Ozone volume mixing ratio (ppmv). (d) Atomic oxygen volume mixing ratio (ppmv).

some in the stratosphere and mesosphere. To explore this, we plotted zonal mean differences of differences between the epoch changes for solar maximum and solar minimum in Figure 6. Most of the structure is probably just due to interannual variability; for instance, there is a signature in the Northern Hemisphere evident of variations in episodic stratospheric warmings, but considerably larger ensembles would be necessary to say anything definitive about that.

4. Conclusion

Models and observations of anthropogenic change in the terrestrial atmosphere show that global mean annual mean temperatures are increasing in the troposphere but decreasing throughout the upper atmosphere. However, above the tropopause, there are also strong solar cycle variations that both confound the analysis of long-term variation and influence its magnitude. There is general agreement between observations and models of the rate of both long-term and solar cycle temperature change as a function of altitude, but some regions lack accurate monitoring over extended time periods, especially the lower thermosphere.

The simulations presented here find that long-term global change in the thermosphere/ionosphere is larger during low solar activity than during high solar activity, but this effect diminishes with decreasing altitude and becomes negligible below the mesopause. The primary reason for this solar cycle dependence of the rate of global change is that CO_2 infrared emission dominates at solar minimum, but at solar maximum, infrared radiation from NO and $O(^3P)$ become a larger fraction of the total radiative cooling budget, so increasing CO_2 has a smaller effect. This effect can be seen from inspection of Figure 7, where we plot global mean annual mean altitude profiles of key gases for solar minimum and solar maximum conditions. Note that cooling by NO is proportional to the product of NO and O, so as solar activity increases, this process is amplified. This is observationally confirmed by data from the Sounding of the Atmosphere using Broad-band Emission Radiometry instrument on the NASA/TIMED satellite (e.g., Mlynczak et al., 2010).

These model experiments were conducted using perpetual solar minimum and solar maximum conditions, in order to simplify the effects of solar activity variation, especially in the thermosphere. In future work, we will perform an extended fully transient run, with time-dependent lower boundary and solar/geomagnetic inputs. Simulations coupled to a dynamical ocean model will also be conducted.

Variations in solar output cause temperature changes throughout the atmosphere, but the most variable regions of the solar spectrum, the ultraviolet, extreme-ultraviolet, and X-ray ranges, are absorbed well above the tropopause. Nevertheless, the theory (e.g., Soon, 2005) that increased solar output has caused the observed increases in temperature in the troposphere and at the surface, during the past century, still has some popular support. That theory is refuted by the fact that the upper atmosphere is cooling. If the cooling is caused by increases in anthropogenic emissions, it is corroborated by the observational evidence and by these modeling studies. If it is caused by decreases in solar activity and solar irradiance, then, a fortiori, the warming of the lower atmosphere must be caused by something else.

Acknowledgments
The authors acknowledge contributions to this work by the many members of the WACCM, CAM, and CESM development teams. As a component of the Community Earth System Model, WACCM-X source code and results are publicly available at http://www.cesm.ucar.edu/. Model output data used in this article are available at https://www2.hao.ucar.edu/modeling/waccm-x. This work was supported by NSF grant 1135432 and by NASA grants NNX14AH54G, NNX15AJ24G, and NNX16AB82G. High-performance computing support from cheyenne (doi:10.5065/D6RX99HX) was provided by the NCAR Computational and Information Systems Laboratory. NCAR is supported by cooperative agreement 1852977 from the National Science Foundation.

References

Akmaev, R. A. (2012). On estimation and attribution of long-term temperature trends in the thermosphere. *Journal of Geophysical Research*, *117*, A09321. https://doi.org/10.1029/2012JA018058

Akmaev, R. A., & Fomichev, V. I. (2000). A model estimate of cooling in the mesosphere and lower thermosphere due to the CO_2 increase over the last 3–4 decades. *Geophysical Research Letters*, *27*(14), 2113–2116. https://doi.org/10.1029/1999GL011333

Akmaev, R. A., Fomichev, V. I., & Zhu, X. (2006). Impact of middle-atmospheric composition changes on greenhouse cooling in the upper atmosphere. *Journal of Atmospheric and Solar Terrestrial Physics*, *68*(17), 1879–1889. https://doi.org/10.1016/j.jastp.2006.03.008

Beig, G., Keckhut, P., Lowe, R. P., Roble, R. G., Mlynczak, M. G., Scheer, J., et al. (2003). Review of mesospheric temperature trends. *Reviews of Geophysics*, *41*(4), 1015. https://doi.org/10.1029/2002RG000121

Brasseur, G., & Hitchman, M. H. (1988). Stratospheric response to trace gas perturbations: Changes in ozone and temperature distributions. *Science*, *240*(4852), 634–637. https://doi.org/10.1126/science.240.4852.634

Cnossen, I., & Richmond, A. D. (2012). How changes in the tilt angle of the geomagnetic dipole affect the coupled magnetosphere-ionosphere-thermosphere system. *Journal of Geophysical Research*, *117*, A10317. https://doi.org/10.1029/2012JA018056

Dickinson, R. E. (1984). Infrared radiative cooling in the mesosphere and lower thermosphere. *Journal of Atmospheric and Terrestrial Physics*, *46*(11), 995–1008. https://doi.org/10.1016/0021-9169(84)90006-0

Emmert, J. T. (2015). Altitude and solar activity dependence of 1967–2005 thermospheric density trends derived from orbital drag. *Journal of Geophysical Research: Space Physics*, *120*, 2940–2950. https://doi.org/10.1029/2015JA021047

Emmert, J. T., Lean, J. L., & Picone, J. M. (2010). Record-low thermospheric density during the 2008 solar minimum. *Geophysical Research Letters*, *37*, L12102. https://doi.org/10.1029/2010GL043671

Emmert, J. T., McDonald, S. E., Drob, D. P., Meier, R. R., Lean, J. L., & Picone, J. M. (2014). Attribution of interminima changes in the global thermosphere and ionosphere. *Journal of Geophysical Research: Space Physics*, *119*, 6657–6688. https://doi.org/10.1002/2013JA019484

Emmert, J. T., Picone, J. M., Lean, J. L., & Knowles, S. H. (2004). Global change in the thermosphere: Compelling evidence of a secular decrease in density. *Journal of Geophysical Research*, *109*, A02301. https://doi.org/10.1029/2003JA010176

Emmert, J. T., Picone, J. M., & Meier, R. R. (2008). Thermospheric global average density trends 1967-2007, derived from orbits of 5000 near-Earth objects. *Geophysical Research Letters*, *35*, L05101. https://doi.org/10.1029/2007GL032809

Eyring, V., Lamarque, J. F., Hess, P., Arfeuille, F., Bowman, K., Chipperfiel, M. P., et al. (2013). Overview of IGAC/SPARC Chemistry-Climate Model Initiative (CCMI) community simulations in support of upcoming ozone and climate assessments. *SPARC Newsletter*, *40*, 48–66.

Fels, S. B., Mahlman, J. D., Schwarzkopf, M. D., & Sinclair, R. W. (1980). Stratospheric sensitivity to perturbations in ozone and carbon dioxide: Radiative and dynamical response. *Journal of Atmospheric Sciences*, *37*(10), 2265–2297. https://doi.org/10.1175/1520-0469(1980)037<2265:SSTPIO>2.0.CO;2

Fomichev, V. I., Jonsson, A. I., de Grandpre, J., Beagly, S. R., McLandress, C., Semeniuk, K., & Shepherd, T. (2007). Response of the middle atmosphere to CO_2 doubling: Results from the Canadian middle atmosphere model. *Journal of Climate*, *20*(7), 1121–1144. https://doi.org/10.1175/JCLI4030.1

Garcia, R. R., Marsh, D. R., Kinnison, D. E., Boville, B. A., & Sassi, F. (2007). Simulation of secular trends in the middle atmosphere, 1950–2003. *Journal of Geophysical Research*, *112*, D09301. https://doi.org/10.1029/2006JD007485

Huang, B., Banzon, V. F., Freeman, E., Lawrimore, J., Liu, W., Peterson, T. C., et al. (2015). Extended reconstructed sea surface temperature version 4 (ERSST.v4). Part I: upgrades and intercomparisons. *Journal of Climate*, *28*(3), 911–930. https://doi.org/10.1175/JCLI-D-14-00006.1

Huang, B., et al. (2017). The climate data guide: SST data—NOAA extended reconstruction SSTs, version 4. Retrieved from https://climatedataguide.ucar.edu/climate-data/sst-data-noaa-extended-reconstruction-ssts-version-4

Hurrell, J. W., Holland, M. M., Gent, P. R., Ghan, S., Kay, J. E., Kushner, P. J., et al. (2013). The community Earth system model: A framework for collaborative research. *Bulletin of the American Meteorological Society*, *94*(9), 1339–1360. https://doi.org/10.1175/BAMS-D-12-00121.1

Keating, G. M., Tolson, R. H., & Bradford, M. S. (2000). Evidence of long-term global decline in the Earth's thermospheric densities apparently related to anthropogenic effects. *Geophysical Research Letters*, *27*(10), 1523–1526. https://doi.org/10.1029/2000GL003771

Laštovička, J. (2017). A review of recent progress in trends in the upper atmosphere. *Journal of Atmospheric and Solar Terrestrial Physics*, *163*, 2–13. https://doi.org/10.1016/j.jastp.2017.03.009

Laštovička, J., Akmaev, R. A., Beig, G., Bremer, J., & Emmert, J. T. (2006). Global change in the upper atmosphere. *Science*, *314*(5803), 1253–1254. https://doi.org/10.1126/science.1135134

Laštovička, J., Solomon, S. C., & Qian, L. (2012). Trends in the neutral and ionized upper atmosphere. *Space Science Reviews*, *168*(1-4), 113–145. https://doi.org/10.1007/s11214-011-9799-3

Liu, H.-L., Bardeen, C. G., Foster, B. T., Lauritzen, P., Liu, J., Lu, G., et al. (2018). Development and validation of the Whole Atmosphere Community Climate Model with thermosphere and ionosphere extension (WACCM-X v. 2.0). *Journal of Advances in Modeling Earth Systems*, *10*, 381–402. https://doi.org/10.1002/2017MS001232

Liu, H.-L., Foster, B. T., Hagan, M. E., McInerney, J. M., Maute, A., Qian, L., et al. (2010). Thermosphere extension of the Whole Atmosphere Community Climate Model. *Journal of Geophysical Research*, *115*, A12302. https://doi.org/10.1029/2010JA015586

Lübken, F.-J., Berger, U., & Baumgarten, G. (2013). Temperature trends in the midlatitude summer mesosphere. *Journal of Geophysical Research: Atmospheres*, *118*, 13,347–13,360. https://doi.org/10.1002/2013JD020576

Marcos, F. A., Wise, J. O., Kendra, M. J., Grossbard, N. J., & Bowman, B. R. (2005). Detection of a long-term decrease in thermospheric neutral density. *Geophysical Research Letters*, *32*, L04103. https://doi.org/10.1029/2004GL021269

Marsh, D. R., Garcia, R. R., Kinnison, D. E., Boville, B. A., Sassi, F., Solomon, S. C., & Matthes, K. (2007). Modeling the whole atmosphere response to solar cycle changes in radiative and geomagnetic forcing. *Journal of Geophysical Research*, *112*, D23306. https://doi.org/10.1029/2006JD008306

Marsh, D. R., Mills, M. J., Kinnison, D. E., Lamarque, J.-F., Calvo, N., & Polvani, L. M. (2013). Climate change from 1850 to 2005 simulated in CESM1 (WACCM), 73727391. *Journal of Climate*, *26*(19), 7372–7391. https://doi.org/10.1175/JCLI-D-12-00558

Mlynczak, M. G., Hunt, L. A., Marshall, B. T., Martin-Torres, F. J., Mertens, C. J., Russell, J. M. III, et al. (2010). Observations of infrared radiative cooling in the thermosphere on daily to multiyear timescales from the TIMED/SABER instrument. *Journal of Geophysical Research*, *115*, A03309. https://doi.org/10.1029/2009JA014713

Neale, R., Richter, J., Park, S., Lauritzen, P., Vavrus, S., Rasch, P., & Zhang, M. (2013). The mean climate of the Community Atmosphere Model (CAM4) in forced SST and fully coupled experiments. *Journal of Climate*, *26*(14), 5150–5168. https://doi.org/10.1175/JCLI-D-12-00236.1

Picone, J. M., Hedin, A. E., Drob, D. P., & Aikin, A. C. (2002). NRLMSISE-00 empirical model of the atmosphere: Statistical comparisons and scientific issues. *Journal of Geophysical Research*, *107*(A12), 1468. https://doi.org/10.1029/2002JA009430

Qian, L., Burns, A. G., Solomon, S. C., & Wang, W. (2017). Carbon dioxide trends in the mesosphere and lower thermosphere. *Journal of Geophysical Research: Space Physics*, *122*, 4474–4488. https://doi.org/10.1002/2016JA023825

Qian, L., Jacobi, C., & McInerney, J. M. (2019). Trends and solar irradiance effects in the mesosphere. *Journal of Geophysical Research: Space Physics*, *124*, 1343–1360. https://doi.org/10.1029/2018JA026367

Qian, L., Laštovička, J., Roble, R. G., & Solomon, S. C. (2011). Progress in observations and simulations of global change in the upper atmosphere. *Journal of Geophysical Research*, *116*, A00H03. https://doi.org/10.1029/2010JA016317

Qian, L., Marsh, D., Merkel, A., Solomon, S. C., & Roble, R. G. (2013). Effect of trends of middle atmosphere gases on the mesosphere and thermosphere. *Journal of Geophysical Research: Space Physics*, *118*, 3846–3855. https://doi.org/10.1002/jgra.5035

Qian, L., Roble, R. G., Solomon, S. C., & Kane, T. J. (2006). Calculated and observed climate change in the thermosphere, and a prediction for solar cycle 24. *Geophysical Research Letters*, *33*, L23705. https://doi.org/10.1029/2006GL027185

Qian, L., & Solomon, S. C. (2012). Thermospheric mass density: An overview of temporal and spatial variations. *Space Science Reviews*, *168*(1-4), 147–173. https://doi.org/10.1007/s11214-011-9810-z

Qian, L., Solomon, S. C., & Roble, R. G. (2014). Secular changes in the thermosphere and ionosphere between two quiet Sun periods. *Journal of Geophysical Research: Space Physics*, *119*, 2255–2262. https://doi.org/10.1002/2013JA019438

Rishbeth, H., & Roble, R. G. (1992). Cooling of the upper atmosphere by enhanced greenhouse gases—Modelling of thermospheric and ionospheric effects. *Planetary and Space Science*, *40*(7), 1011–1026. https://doi.org/10.1016/0032-0633(92)90141-A

Roble, R. G., & Dickinson, R. E. (1989). How will changes in carbon dioxide and methane modify the mean structure of the mesosphere and thermosphere? *Geophysical Research Letters*, *16*(12), 1441–1444. https://doi.org/10.1029/GL016i012p01441

Saunders, A., Lewis, H., & Swinerd, G. (2011). Further evidence of long-term thermospheric density change using a new method of satellite ballistic coefficient estimation. *Journal of Geophysical Research*, *116*, A00H10. https://doi.org/10.1029/2010JA016358

She, C.-Y., Krueger, D. A., & Yuan, T. (2015). Long-term midlatitude mesopause region temperature trend deduced from quarter century (1990–2014) Na lidar observations. *Annales Geophysicae*, *33*(3), 363–369. https://doi.org/10.5194/angeocom-33-363-2015

Solomon, S. C., Liu, H.-L., Marsh, D. R., McInerney, J. M., Qian, L., & Vitt, F. M. (2018). Whole atmosphere simulation of anthropogenic climate change. *Geophysical Research Letters*, *45*(3), 1567–1576. https://doi.org/10.1002/2017GL076950

Solomon, S. C., Qian, L., & Burns, A. G. (2013). The anomalous ionosphere between solar cycles 23 and 24. *Journal of Geophysical Research: Space Physics*, *118*, 6524–6535. https://doi.org/10.1002/jgra.50561

Solomon, S. C., Qian, L., Didkovsky, L. V., Viereck, R. A., & Woods, T. N. (2011). Causes of low thermospheric density during the 2007–2009 solar minimum. *Journal of Geophysical Research*, *116*, A00H07. https://doi.org/10.1029/2011JA016508

Solomon, S. C., Qian, L., & Mannucci, A. J. (2018). Ionospheric electron content during solar cycle 23. *Journal of Geophysical Research: Space Physics*, *123*, 5223–5231. https://doi.org/10.1029/2018JA025464

Solomon, S. C., Qian, L., & Roble, R. G. (2015). New 3D simulations of climate change in the thermosphere. *Journal of Geophysical Research: Space Physics*, *120*, 2183–2193. https://doi.org/10.1002/2014JA020886

Solomon, S. C., Woods, T. N., Didkovsky, L. V., Emmert, J. T., & Qian, L. (2010). Anomalously low solar extreme-ultraviolet irradiance and thermospheric density during solar minimum. *Geophyical. Research Letters*, *37*, L16103. https://doi.org/10.1029/2010GL044468

Soon, W. W.-H. (2005). Variable solar irradiance as a plausible agent for multidecadal variations in the Arctic-wide surface air temperature record of the past 130 years. *Geophysical Research Letters*, *32*, L16712. https://doi.org/10.1029/2005GL023429

Wang, W., & Qian, L. (2018). Trend in ionospheric temperatures. Paper presented at the TREND-2018 workshop, Hefei, China.

Yuan, T., She, C.-Y., & Krueger, D. A. (2018). The long-term variations of nocturnal mesopause temperature and altitude revealed by the Na lidar observations between 1990 and 2017 at mid-latitude. Paper presented at the TREND-2018 workshop, Hefei, China, 2018.

Zhang, S.-R., & Holt, J. M. (2013). Long-term ionospheric cooling: Dependency on local time, season, solar activity, and geomagnetic activity. *Journal of Geophysical Research: Space Physics*, *118*, 3719–3730. https://doi.org/10.1002/jgra.50306

Zhang, S.-R., Holt, J. M., Erickson, P. J., Goncharenko, L. P., Nicolls, M. J., McCready, M., & Kelly, J. (2016). Ionospheric ion temperature climate and upper atmospheric long term cooling. *Journal of Geophysical Research: Space Physics*, *121*, 8951–8968. https://doi.org/10.1002/2016JA022971

Zhang, S.-R., Holt, J. M., & Kurdzo, J. (2011). Millstone Hill ISR observations of upper atmospheric long-term changes: Height dependency. *Journal of Geophysical Research*, *116*, A00H05. https://doi.org/10.1029/2010JA016414